Chemistry Europe
European Chemical Societies Publishing

WILEY VCH

Excellence in Chemistry Research



Announcing our new flagship journal

- Gold Open Access
- Publishing charges waived
- Preprints welcome
- Edited by active scientists

Meet the Editors of *ChemistryEurope*



Luisa De Cola
Università degli Studi di Milano Statale, Italy



Ive Hermans
University of Wisconsin-Madison, USA



Ken Tanaka
Tokyo Institute of Technology, Japan

Check for updates

ChemistrySelect

Research Article
doi.org/10.1002/slct.202300910

Chemistry Europe
European Chemical Societies Publishing

www.chemistryselect.org

Focusing on New Piperazinyl-methyl-3(2*H*)pyridazinone Based Derivatives: Design, Synthesis, Anticancer Activity and Computational Studies

İrem Bozbey Merde,[a] Gülce Taşkor Önel,[b] Senem Akkoç,[c, d] Zeynep Karaköy,[e] and Burçin Türkmenoğlu*[b]

Heterocyclics containing pyridazinone and piperazine structures are potential anticancer agents in the treatment of cancer disease caused by increasing the number of abnormal cells disrupting body biochemistry. There is a need for the design of more biocompatible drugs for the treatment of cancer with minimal side effects. For this purpose, a series of piperazinyl-methyl-3(2*H*)pyridazinone based compounds were synthesized and their anticancer activities were studied *in vitro* and *in silico*. The chemical structures of all the new compounds **3** (**a**–**k**) were identified by spectral analysis. The new compounds were screened in human lung and colon cancer cell lines to learn about their cytotoxic effects. The importance of the structure activity relationship was seen in this study and the compounds containing methoxy groups on the phenyl ring (**3 a**, **3 b**, **3 e**–**3 g**) were found to have higher cytotoxic effects than those without. It was determined that one of these compounds (**3 a**) demonstrated significant cytotoxic effect against both cell lines for 72 h as *in vitro*. The geometry of the synthesized **3 a** ligand was optimized using the hybrid B3LYP functional density functional theory (DFT). Molecular docking study of **3 a** compound was performed against EGFR (PDB ID : 1M17) and VEGFR-2 (PDB ID: 2RL5) molecular targets.

Introduction

Cancer is a disease in which abnormal or damaged cells grow and multiply uncontrollably and spread to other parts of the body. It is a multifactorial disease that is one of the leading causes of death worldwide and occurs in parallel with genetic, epigenetic, and environmental factors. Cancer consists of millions of cells and can start almost anywhere in the human body. For this reason, the number of cancer patients is expected by the World Health Organization to reach 22 million by 2030.[1] The aim of research in this area is to develop anticancer drugs with high efficacy and low toxicity.[2]

Lung cancer is one of the malignant tumors with a high incidence and mortality.[3] To date, various diagnostic and therapeutic strategies have been applied for lung cancer. Despite this, the survival rates of lung cancer patients are still very low.[4] Colorectal cancer (CRC) is one of the most common types of cancer worldwide. Although expressed as colon cancer, it includes all cancers that begin in the colon and rectum. CRC is the third most diagnosed cancer with an estimated 1–2 million new cases worldwide each year. Despite advances in treatment, one of the main reasons for the high mortality in these cancer types is the failure of current treatment options. Because in cancers such as CRC, surgical intervention can be performed in the early stages. The efficacy and response rates of current chemotherapy agents are still very low.[5]

The piperazine ring is a structural fragment found in many pharmacologically active compounds. It has been reported in the literature that many compounds with a piperazine ring act as cytotoxic agents against cancer cells. Naftopidil (**3**), gilteritinib (**4**) and a lot of aryl piperazines (**1**, **2**) have demonstrated potent antiproliferative activity against many cancer cells, including colon, breast, lung, and leukemia.[6]

The pyridazinone base ring and its chemistry have been an interesting area of study that has been studied extensively in recent years.[7] The synthesis of new pyridazinone derivative compounds and the investigation of the biological activities of these structures have gained great importance in recent years. When the literature is examined, it is seen that pyridazinones have many pharmacological effects. Substituted pyridazinones show pharmacological effects such as antidepressant, antihy-

[a] *Dr. İ. B. Merde*
Department of Pharmaceutical Chemistry,
Faculty of Pharmacy,
Erzincan Binali Yıldırım University,
Yalnızbağ, 24002 Erzincan, Turkey
[b] *Dr. G. T. Önel, Dr. B. Türkmenoğlu*
Department of Analytical Chemistry,
Faculty of Pharmacy,
Erzincan Binali Yıldırım University,
Yalnızbağ, 24002 Erzincan, Turkey
E-mail: burcin.turkmenoglu@erzincan.edu.tr
[c] *Dr. S. Akkoç*
Department of Basic Pharmaceutical Sciences,
Faculty of Pharmacy,
Suleyman Demirel University,
32260 Isparta, Turkey
[d] *Dr. S. Akkoç*
Faculty of Engineering and Natural Sciences,
Bahçeşehir University,
34353 Istanbul, Turkey
[e] *Z. Karaköy*
Department of Pharmacology,
Faculty of Pharmacy,
Erzincan Binali Yıldırım University,
24002 Yalnızbağ Erzincan, Turkey

Supporting information for this article is available on the WWW under https://doi.org/10.1002/slct.202300910

© 2023 Wiley-VCH GmbH

pertensive, anticonvulsant, cardiotonic, antibacterial, cholinesterase inhibitor, diuretic, anti-HIV and anticancer (**1**, **5**, **6**).[8]

Based on the therapeutic activities of pyridazinone and piperazine derivatives, compounds with anticancer and antiproliferative effects with a pyridazinone ring and naftopidil with a piperazine ring and derivatives with reported anticancer activities in the literature were investigated. Accordingly, in this study, new compounds containing pyridazinone and piperazine rings, which are two important ring systems, were designed and synthesized (Figure 1). Biological activities of synthesized piperazine derivative compounds were evaluated, *in silico* studies, DFT calculations, HOMO-LUMO energies, conformer calculations, and spectral analyzes were examined.

Results and Discussion

Chemistry

The starting materials were obtained by the acid-catalysed aldol condensation with glyoxylic acid and nucleophilic substitution reaction with hydrazide. A Mannich Reaction of substituted pyridazinone with monosubstituted piperazines in the presence of aqueous formaldehyde was used to synthesize new piperazinyl-methyl-3(2*H*)pyridazinone based derivatives. (Scheme 1) The synthesized products were in white solid form and the yields ranged from 28–78 %. The ^{1}H NMR spectra of the pyridazinone group protons were observed in the range of 8.02–7.97 ppm and 7.04–6.47 ppm with two characteristic doublet signals stated *J*-coupling constant 8 Hz. The range of 3.66–2.93 ppm and 3.18–2.64 ppm in the ^{1}H NMR spectrum showed the two triplet signals of piperazine group protons. In addition, the anisole or *p*-tolyl groups and *N*-substituted aromatic rings attached to piperazine were observed in the arene region in the range of 7.8–6.7 ppm. In the ^{13}C NMR spectrum, the pyridazinone ring carbonyl carbon supported the structure accuracy in the range of 158.4–160.7 ppm. In the IR spectra, newly synthesized compounds **3 (a–k)** exhibited characteristic ν(C=O) bands at 1661–1648 cm^{-1} for pyridazinone rings. The monographs of all compounds **3 (a–k)** were processed below.

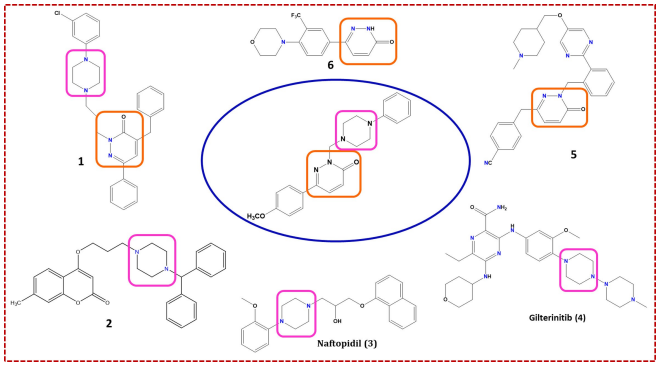


Figure 1. Design of target compounds (**3 a–3 k**).

Biological evaluation and structure-activity relationship

The synthesized nine new compounds and a positive control drug were evaluated at different concentrations ranging from 200 μM to 6.25 μM for cytotoxic activity against lung and colon cancer cell lines (A549, DLD-1) for 72 hours using the MTT assay method (Table 1).

When the compounds tested against the A549 cell line are evaluated as general, it is seen in Table 1 that the compounds containing methoxy group at the para position of the phenyl ring (**3 a**, **3 b**, **3 e–3 g**) have higher cytotoxic effects than the compounds containing methyl group at the para position of the phenyl ring (**3 h–3 k**). In fact, all of the compounds containing the methyl group (**3 h–3 k**) were found to be inactive against the lung cancer cell line with IC_{50} values higher than 200 μM. All of the compounds containing the methoxy group (**3 a**, **3 b**, **3 e–3 g**) show that they inhibit the growth of lung cancer cells with IC_{50} values ranging from 36.79 μM to 199.3 μM and give antiproliferative effect on this cell line. Among these compounds, it was observed that compound **3 a**, which contain phenyl ring on the para position of piperazine ring attached to pyridazinone, gave the highest activity. For compound **3 b**, it was observed that when 4-methyl phenyl instead of phenyl was attached to the same ring, the cytotoxic activity decreased to 149.70 μM. Thus, it can be clearly seen in this study that the structure of the synthesized molecules plays an important role on the biological activity.

Except for one of the compounds synthesized (**3 h**) against colon cancer cells, all of the other compounds (**3 a**, **3 b**, **3 e–3 g**, **3 i**, **3 j**, **3 k**) were found to have cytotoxic effects and their IC_{50} values were obtained between 34.84 μM and 186.0 μM. In this cell line, as in the lung cell line, it was determined that the compounds containing methoxy group at the 4 positions of the phenyl ring (**3 a**, **3 b**, **3 e–3 g**) showed higher antiproliferative effects than those containing methyl group (**3 h–3 k**). It was identified that the compound **3 h**, which contains a methyl group on the phenyl ring and a 4-fluorophenyl substituent on the piperazinyl ring, did not show cytotoxic effects in both cell lines and was inactive. Compounds **3 b** and **3 e** showed very close cytotoxic effects against colon cancer cell line with IC_{50} values of 94.27 and 97.22 μM, respectively. While three compounds (**3 i**, **3 j**, **3 k**) did not show activity on cancerous lung cells, they inhibited the growth of colon cancer cells and

Table 1. IC_{50} values of compounds.

Compounds	IC_{50} (μM) A549	DLD-1
3 a	**36.79**	**34.84**
3 b	149.70	94.27
3 e	199.30	97.22
3 f	122.10	107.00
3 g	141.80	137.80
3 h	> 200	> 200
3 i	> 200	156.50
3 j	> 200	186.00
3 k	> 200	140.50
Cisplatin	20.05	17.11

© 2023 Wiley-VCH GmbH

23656549, 2023, 25, Downloaded from https://chemistry-europe.onlinelibrary.wiley.com/doi/10.1002/slct.202300910 by Erzincan Universitesi, Wiley Online Library on [10/07/2023]. See the Terms and Conditions (https://onlinelibrary.wiley.com/terms-and-conditions) on Wiley Online Library for rules of use; OA articles are governed by the applicable Creative Commons License

23656549, 2023, 25, Downloaded from https://chemistry-europe.onlinelibrary.wiley.com/doi/10.1002/slct.202300910 by Erzincan Universitesi, Wiley Online Library on [10/07/2023]. See the Terms and Conditions (https://onlinelibrary.wiley.com/terms-and-conditions) on Wiley Online Library for rules of use; OA articles are governed by the applicable Creative Commons License

were determined by the IC_{50} values calculated. None of the synthesized compounds showed higher efficacy against A549 and DLD-1 cell lines than cisplatin, a clinically used platinum-based drug. However, in these cell culture studies conducted for 72 hours, two compounds (**3a** and **3b**) with high efficacy were selected and were tested against colon cancer cell line for 48 hours with the positive control drug under the same experimental conditions. The IC_{50} values of these compounds (**3a** and **3b**) and cisplatin tested at 200–12.5 μM concentrations (200, 100, 50, 25, 12.5 μM) were found to be 75.40, 120.60 and 70.95 μM, respectively. Antiproliferative activities of compound **3a** and cisplatin tested for 48 hours were seen to be close to each other. We also evaluated compound **3a**, which we found to have the highest efficacy in this study, against liver cancer cell line (HepG2) at five different concentrations (200–12.5 μM) for 48 hours. The IC_{50} value of compound **3a** was obtained as 85.82 μM in HepG2.

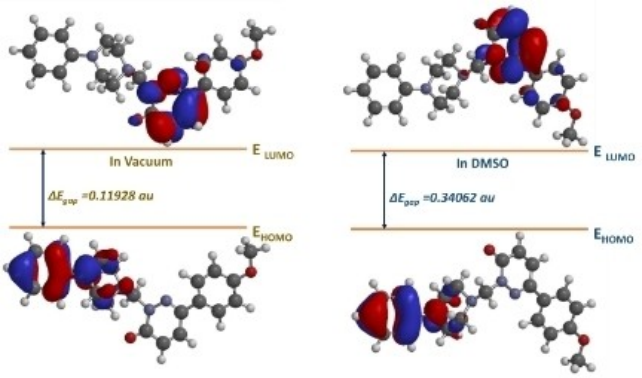


Figure 2. Energy gap values and frontier molecular orbitals of compound **3a** in DMSO and vacuum environment.

Computational Studies

Analysis of frontier molecular orbital

The frontier molecular orbital properties of compound **3a** in different solvents were investigated using the DFT method on B3LYP with 6-311G* base set in Spartan'08 package program.[9] The HOMO and LUMO energy levels and the energy band gap of the compound are very important factors in determining whether there is an efficient charge transfer between the donor and the acceptor.[10]

A higher energy HOMO indicates that a compound will be more reactive in chemical reactions with electrophiles, and a correspondingly lower LUMO energy for chemical reactions with nucleophiles.[11] The gap between HOMO and LUMO determines the stability of the compound in the given medium. As the gap between HOMO and LUMO increases, it indicates the stability of the compound. Low chemical softness and higher hardness support this information. Chemical potential is the tendency of an electron to escape from a stable molecule. A negative chemical potential means the complex is stable and will not spontaneously decompose into elements. Hardness indicates resistance to changes in electron distribution in molecules.[11]

Figure 2 presents the surfaces of HOMO and LUMO of compound **3a** in different environments, while describing the energy gap between HOMO-LUMO.

E_{HOMO}, E_{LUMO}, ΔE_{gap}, chemical hardness, chemical potential, electrophilicity index, chemical softness parameters of all compounds are shown in Table 2. These parameter values were calculated separately for both the DMSO environment and the vacuum environment. Electronic absorption is concerned with the transition from the ground to the first excited state to the LUMO and is mainly defined by an electron excitation from the HOMO.[12] Chemical hardness, softness and chemical potential values vary depending on HOMO-LUMO and its participation in the reaction is interpreted accordingly.

The parameter values in Table 2 are important quantum global chemical descriptors of the molecules studied for their reactivity. In terms of chemical hardness, large ΔE_{gap} indicates hard molecules, small ones indicate soft molecules.

When the results presented in Table 2 were examined, it was determined that almost all calculated quantum descriptors gave results in supported with the experimental IC_{50} data for compound **3a**. The energy range, which is one of the most important parameters determining chemical reactivity, is 0.119279777 au for ΔE_{gap} **3a** compound. This is one of the best values presented in Table 2 and supports the *in vitro* study in Table 1.

The values obtained for the electrophilicity index (ω) are not in the same order. This indicates the unexpected general electrophilic nature of these molecules as a measure of the energy reduction due to the maximum electron flow between the donor and acceptor.[13] The chemical reactivity relationships of these derivatives were determined using DFT methods through local reactivity descriptors such as electrophilic, electronegativity, softness, hardness and chemical potential.[11]

Molecular Docking Studies

In silico approaches, both the interactions at the binding site and the binding parameter values are important. In this study, both parameters were investigated for each crystal structure. Analysis of compound **3a** to EGFR and VEGFR-2 receptors was performed. Since **3a** compound showed the best results *in vitro* studies, **3a** compound was interacted in molecular docking. While calculating these interactions, they were evaluated in terms of binding interactions with molecular docking studies using Schrödinger 2021-2 software. The 3D crystal structures of EGFR (PDB ID:1M17)[14] and VEGFR-2 (PDB ID:2RL5)[15] were obtained from the protein database, respectively.

In Table 3, the interactions of the co-ligand and **3a** compound on EGFR, VEGFR-2 receptors are given. The **3a** compound, which interacts as *in silico* with EGFR and VEGFR-2 crystal structures, has been shown with docking score, XP Gcore, Glide Score, Glide Energy, Glide Emodel and ΔG_{Bind} energy values.

© 2023 Wiley-VCH GmbH

Table 2. E_{HOMO}, E_{LUMO}, ΔE_{gap}, chemical hardness, chemical potential, electrophilicity index, chemical softness energies of compounds **3(a–k)**

VACUUM	3a	3b	3c	3d	3e	3f	3g	3h	3i	3j	3k
E_{HOMO} (au)	−0.191490758	−0.186698217	−0.228018964	−0.197135463	−0.2025673	−0.204255928	−0.211116584	−0.211515745	−0.206564054	−0.205414065	−0.194600236
E_{LUMO} (au)	−0.072210981	−0.071879654	−0.076743016	−0.053228267	−0.067092342	−0.070041137	−0.071694904	−0.073516419	−0.071556035	−0.071078895	−0.075277525
$E_{LUMO-LUMO}$ (ΔE_{gap}) (au)	0.119279777	0.114818563	0.151275948	0.143907196	0.135474958	0.134214791	0.13942168	0.137999326	0.135008019	0.13433517	0.119322711
Chemical hardness (au)	0.059639889	0.057409281	0.075637974	0.071953598	0.067737479	0.067107395	0.06971084	0.068999663	0.06750401	0.067167585	0.059661355
Chemical potential (au)	−0.131850869	−0.129288936	−0.15238099	−0.125181865	−0.134829821	−0.137148533	−0.141405744	−0.142516082	−0.139060044	−0.13824648	−0.134938881
Electrophilicity index (au)	0.008692326	0.008357814	0.011609983	0.00783525	0.00908954	0.00940486	0.009997792	0.010155417	0.009668848	0.009556045	0.009104251
Chemical softness (au)	16.76730159	17.41878621	13.22087238	13.89784564	14.762876	14.90148731	14.34497135	14.49282443	14.81393483	14.8881339	16.76126854
DMSO	3a	3b	3c	3d	3e	3f	3g	3h	3i	3j	3k
E_{HOMO} (au)	−0.278475345	−0.274101847	−0.302809481	−0.286490171	−0.298162222	−0.297772212	−0.211116584	−0.307103642	−0.30575509	−0.305290652	−0.287277936
E_{LUMO} (au)	0.055872281	0.055869983	0.051537373	0.052656173	0.057959555	0.056781612	0.055485115	0.055086095	0.057151841	0.057312081	0.053884666
$E_{LUMO-LUMO}$ (ΔE_{gap}) (au)	0.334347626	0.32997183	0.354346854	0.339146344	0.356121777	0.354553824	0.266601699	0.362189737	0.362906931	0.362602733	0.341162602
Chemical hardness (au)	0.167173813	0.164985915	0.177173427	0.169573172	0.178060888	0.177276912	0.133300849	0.181094869	0.181453466	0.181301367	0.170581301
Chemical potential (au)	−0.111301532	−0.109115932	−0.125636054	−0.116916999	−0.120101334	−0.1204953	−0.077815735	−0.126008773	−0.124301625	−0.123989285	−0.116696635
Electrophilicity index (au)	0.006194016	0.005953143	0.007892209	0.006834792	0.007212165	0.007259559	0.003027644	0.007939105	0.007725447	0.007686671	0.006809052
Chemical softness (au)	5.981798116	6.061123456	5.64418726	5.897159255	5.616056449	5.640892475	7.501827675	5.521967617	5.511054844	5.515678227	5.862307263

Table 3. Binding energy values of co-ligand, **3a**-EGFR (1M17), co-ligand, **3a**-VEGFR-2 (2RL5) interactions.

Parameters	EGFR (PDB ID:1 M17)		VEGFR-2 (PDB ID:2RL5)	
	3a	Co-ligand	**3a**	Co-ligand
Docking Score	−4.861	−9.843	−5.363	−10.648
XP GScore	−6.406	−9.843	−6.908	−11.513
Glide Score	−6.406	−9.843	−6.908	−11.513
Glide Energy	−43.448	−57.609	−48.215	−73.302
Glide Emodel	−53.935	−76.509	−70.163	−107.85
ΔG_{Bind}	−58.69	−83.69	−66.45	−114.26

Table 3, primarily when analyzed for interactions between EGFR and **3a** compounds, the value of the XP Gscore value (−9.843 kcal/mol) is better than the value of the compound **3a** (−6.406 kcal/mol).

In addition, it can be said that the values of co-Ligand and **3a** are close to each other when the free connection energy values are compared to the EGFR receptor.

In the same way, when Table 3 analyzed for VEGFR-2, calculations were applied for co-ligand and **3a** of the binding parameter values. The ΔG_{Bind} energy value of the **3a** compound interaction with VEGFR-2 is −66.45 kcal/mol, and co-ligand's ΔG_{Bind} energy value is −114.26 kcal/mol.

Figure 3 presented 2D and 3D interaction diagrams of the **3a** compound interacting with EGFR and *in silico*. The presence of hydrogen bond was determined by Met769, which is important amino acid to EGFR. It has also been determined that EGFR is docked in the active binding site.

The interaction diagram of VEGFR-2-**3a** complex is presented in Figure 4. It has been determined that the compound **3a**, one of the important amino acids of the active binding zone, was docked by the Cys919 and hydrogen bond interaction, and by Lys868, Glu885, Asp1046 amino acids.

While the studies in molecular docking are applied, the ligands in the crystal structure are compared with the compounds synthesized and *in vitro* studies. When Figure 5 was analyzed, it was understood that the compound of co-Ligands and **3a** is connected from the similar part of the receptors.

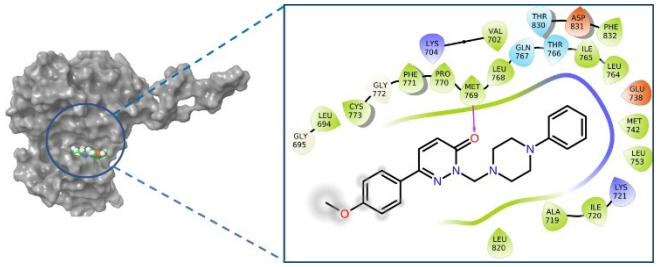


Figure 3. 2D and 3D interaction diagram of the 3a compound interacting with EGFR crystal structure (PDB ID:1M17).

© 2023 Wiley-VCH GmbH

23656549, 2023, 25, Downloaded from https://chemistry-europe.onlinelibrary.wiley.com/doi/10.1002/slct.202300910 by Erzincan Universitesi, Wiley Online Library on [10/07/2023]. See the Terms and Conditions (https://onlinelibrary.wiley.com/terms-and-conditions) on Wiley Online Library for rules of use; OA articles are governed by the applicable Creative Commons License

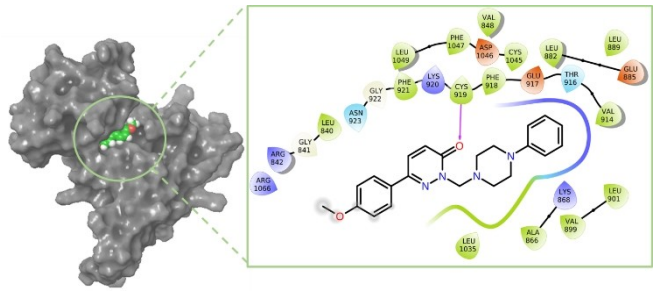


Figure 4. 2D and 3D interaction diagram of the 3a compound interacting with VEGFR-2 crystal structure (PDB ID:2RL5).

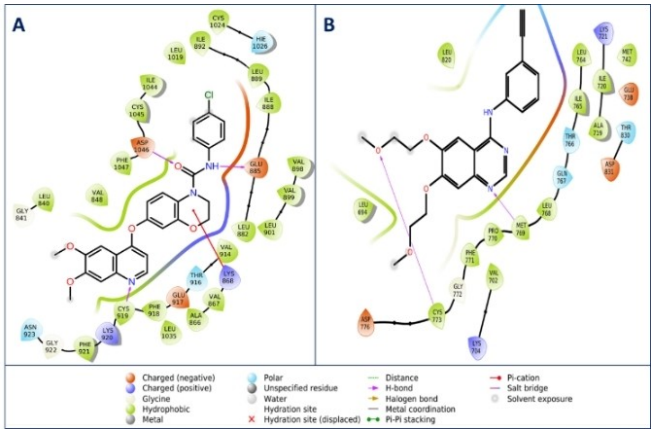


Figure 5. (a) 2D interaction diagram of co-ligand interaction with EGFR crystal structure (PDB ID:1M17). (b) 2D interaction diagram of co-ligand interaction with VEGFR-2 crystal structure (PDB ID:2RL5).

ADMET Prediction

The absorption, distribution, metabolism, excretion, and toxicity (ADMET) of the compounds that may be drug candidates are preferred in drug design recently. ADMET parameter values were estimated using Schrödinger 2021-2 Qikprop wizard *in silico* approaches. The pharmacokinetic profile of these compounds is presented in Table 4 of QPlogBB, QPlogPo/w QPPCaco, QPlogHERG, QPPMDCK, QPlogKHSA, RuleofFive.

ADMET parameters for all synthesized compounds were determined to be within the acceptable range defined for human use. This presents its positive pharmacokinetic profile.

Conclusion

In summary, this is the first paper on the synthesis and spectroscopic characterization of novel piperazinyl-methyl-3(2*H*)pyridazinone based compounds **3(a–k)** in satisfactory yields, as well as evaluation of their potential anticancer activities *in vitro* and *in silico* studies. The anticancer activity profiles of the piperazinyl-pyridazinone analogues **3a** suggest that these derivatives could be further investigated as a template for the synthesis of promising piperazinyl-pyridazinone derivatives with fewer side effects and better cancer cell inhibitory effects. The anticancer activity profiles of the piperazinyl-pyridazinone analogs **3a** suggest that these derivatives could be further investigated as a hopeful formwork for the synthesis of promising piperazinyl-pyridazinone derivatives with fewer side effects and better cancer cell inhibitory effects. The synthesized compounds were tested *in vitro* against two different human cancer cell lines including lung and colon. Among the tested compounds, it was determined that the compounds containing methoxy group on the phenyl ring (**3a**, **3b**, **3e**–**3g**) showed high activity against both types of cancer. It was seen that one of the compounds (**3a**) had the highest cytotoxic effect against both cell lines with IC_{50} values of 36.79 and 34.84 μM, respectively. It has been understood from the results of the study that computational approaches including molecular docking and DFT results are supported of *in vitro* studies. It was determined that the free binding energy calculated according to the MM-GBSA method for the compound with the best activity value (**3a**) docked on the EGFR and VEGR-2 targets. When the results presented according to the DFT method in Table 2 are examined, almost all the calculated quantum descriptors are supportive with the

Table 4. ADMET parameters for all synthesized compounds.

Com.	QPlogBB[a]	QPlogPo/w[b]	QPlogHERG[c]	QPPCaco[d]	QPPMDCK[e]	QPlogKhsa[f]	Rule of five[g]
3a	0.184	4.122	−7.283	793.111	109.490	0.496	0
3b	0.203	4.414	−7.078	835.039	450.406	0.648	0
3c	0.491	5.130	−7.290	868.297	2070.300	0.765	1
3d	0.350	4.628	−7.196	796.165	1056.600	0.624	0
3e	0.442	3.749	−7.980	194.145	104.678	0.457	0
3f	0.515	3.590	−8.049	259.732	141.020	0.261	0
3g	0.565	3.665	−7.949	196.245	188.471	0.331	0
3h	0.630	3.928	−7.948	198.185	190.487	0.527	0
3i	0.493	3.998	−7.969	193.311	102.479	0.652	0
3j	0.438	3.758	−7.989	195.931	103.981	0.461	0
3k	0.385	4.625	−7.217	851.697	833.003	0.730	0

[a] Predicted blood brain barrier permeability (−3 to 1.2) [b] Predicted octanol/water partition coefficient (−2.0 to 6.5) [c] Predicted IC50 value for blockage of HERG K+channels (< −5.0) [d] Permeability in Caco cell assay, model for intestinal absorption (< 25-low; > 500-high) [e] Predicted apparent MDCK cell permeability in nm/s (acceptable range in nm/s (acceptable range: < 25 is poor and > 500 is great) [f] Prediction of binding to human serum albumin (−1.5 to 1.5) [g] Lipinski rule of five.

© 2023 Wiley-VCH GmbH

23656549, 2023, 25, Downloaded from https://chemistry-europe.onlinelibrary.wiley.com/doi/10.1002/slct.202300910 by Erzincan Universitesi, Wiley Online Library on [10/07/2023]. See the Terms and Conditions (https://onlinelibrary.wiley.com/terms-and-conditions) on Wiley Online Library for rules of use; OA articles are governed by the applicable Creative Commons License

experimental IC_{50} data for compound **3a**. In addition, the properties of the compounds synthesized by ADME studies were determined and their ranges within the determined reference values are presented in Table 4. Molecular docking studies of compound **3a**, which was synthesized and had high *in vitro* activity, were applied by interacting with two different receptors. The binding parameter values of compound **3a**, which interacts with both EGFR and VEGFR-2, and amino acids in the binding site were determined. The pharmacokinetic properties of all synthesized compounds were calculated by Schrödinger ADMET estimation. According to both experimental and computational results, it can be suggested that the compounds whose anticancer properties are investigated are candidates for AChE and drug research.

Experimental Section

Synthesis

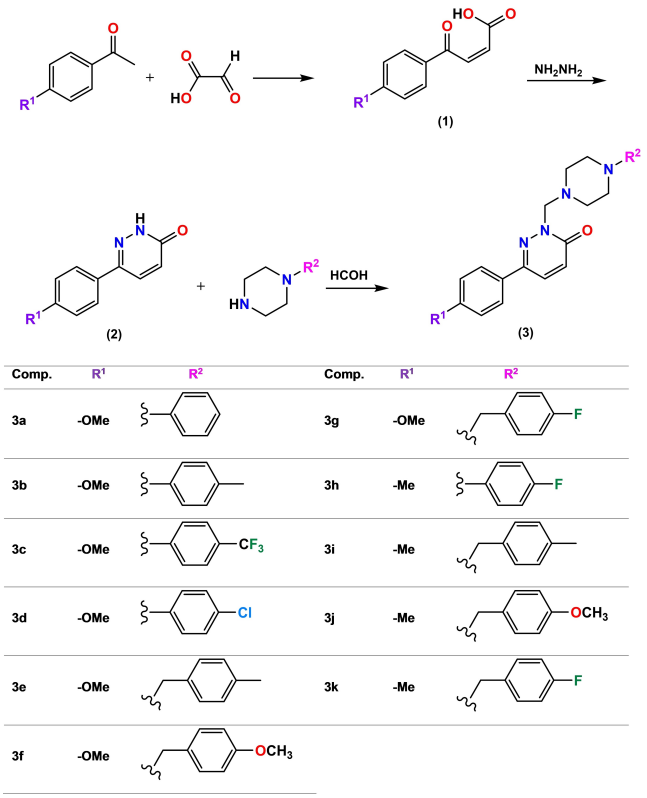
Unless otherwise noted, all of the reagents were commercial quality and were used without purification. The progress of reactions and the purity of the compounds were monitored by TLC using silica gel plates (250 μm, F_{254}) under UV light. NMR spectra were recorded on a Bruker Ultrashield Plus Biospin Avance III 400 MHz NaNoBay FT NMR (^{1}H, 400 MHz; ^{13}C, 100 MHz), in DMSO-d_6 (internal standard tetramethylsilane). Chemical shifts (δ) are expressed as parts per million (ppm) downfield from tetramethylsilane (TMS) and the coupling constants (J) quoted in Hertz. Splitting patterns have been designated as follows: s (singlet), d (doublet), dd (doublet of doublets), t (triplet) and m (multiplet), br (broad). The IR Spectra were recorded on Thermo Scientific Nicolet 6700 ATR/Fourier transform infrared spectrophotometer. Naming of products was done using PerkinElmer ChemDraw Ultra 18.1.0.535.

General procedure for the preparation of compounds (1) and (2)

The substituted-acetophenone (1 mmol), glyoxylic acid monohydrate (1 mmol), and acetic acid (2 mL) were heated and stirred under reflux for 5 h. After the reaction was completed, the reaction mixture cooled down to room temperature, and 20 mL of water and ammonium hydroxide solution (25%) were added until the medium pH became 8. Then the reaction mixture was extracted with dichloromethane (3×20 mL). To the aqueous layer was added hydrazine hydrate (10 mmol) and the reaction mixture was refluxed for 3 h. After completion of the reaction, the reaction mixture cooled down to room temperature. The resulting white precipitate was filtered and used for the next step without further purification.[16]

General procedure for the preparation of compounds 3(a–k)

A solution of 35% aqueous formaldehyde (1 mmol) and compound 2 (1 mmol) in EtOH (15 mL) were refluxed for 12 h with continuous stirring. After the reaction is completed, the crude was evaporated under reduced pressure. The oily residue was triturated with diethyl ether, and the resulting solid was collected by filtration and recrystallized from EtOH:Diethyl ether (2:3).[17] Compounds **3** (**a**–**k**) were obtained shown in Scheme 1.



Comp.	R^1	R^2	Comp.	R^1	R^2
3a	-OMe		3g	-OMe	F
3b	-OMe		3h	-Me	F
3c	-OMe	CF_3	3i	-Me	
3d	-OMe	Cl	3j	-Me	OCH_3
3e	-OMe		3k	-Me	F
3f	-OMe	OCH_3			

Scheme 1. Synthesis of piperazinyl-methyl-3(2*H*)pyridazinone based compounds **3** (**a**–**k**).

Biological studies

Cytotoxic activity studies were conducted according to the procedure in previous studies[18] Human colon cancer cell line (DLD-1; ATCC® CCL-221™), human lung cancer cell line (A549; ATCC® CCL-185™) were purchased from the American Type Culture Collection (ATCC, USA). Cells were cultured in Dulbecco's modified Eagle's Medium-high-glucose supplemented with 10% fetal bovine serum and %1 glutamax. The cell seeding was done at a density of 5×10^3 cells/well into sterile 96-well plates. The DLD-1 and A549 cells were exposed to the compounds at different concentrations (200, 100, 50, 25, 12.5 and 6.25 μM) for 72 h. The MTT solution was added to each well in the plates and they were incubated for an additional 2 h. Absorbance values were measured in Elisa plate reader device at 590 nm, and IC_{50} values were calculated by GraphPad Prism Software 5.

Computational Details

Molecular modelling aims to represent or understand the behaviour of molecules using all computational methods.[19] Computational studies were carried out in three parts. For this, the synthesized compound with the best cytotoxic activity was used in the calculations. First, the geometric optimization of the **3a** compound with the best cytotoxic activity was performed using the B3LYP/6-311G theory level DFT calculations in the Spartan'08 package program. In the second part, molecular docking investigations were carried out *in silico*. As the last part, the ADME properties of all synthesized compounds were calculated with the Schrödinger 2021-2 QikPrep interface.

© 2023 Wiley-VCH GmbH

23656549, 2023, 25, Downloaded from https://chemistry-europe.onlinelibrary.wiley.com/doi/10.1002/slct.202300910 by Erzincan Universitesi, Wiley Online Library on [10/07/2023]. See the Terms and Conditions (https://onlinelibrary.wiley.com/terms-and-conditions) on Wiley Online Library for rules of use; OA articles are governed by the applicable Creative Commons License

23656549, 2023, 25, Downloaded from https://chemistry-europe.onlinelibrary.wiley.com/doi/10.1002/slct.202300910 by Erzincan Universitesi, Wiley Online Library on [10/07/2023]. See the Terms and Conditions (https://onlinelibrary.wiley.com/terms-and-conditions) on Wiley Online Library for rules of use; OA articles are governed by the applicable Creative Commons License

DFT Studies

The study of molecular orbital and molecular electrostatic properties is the most widely used in the quantum mechanical methods of computational chemistry. Geometry optimization and modification of the compounds investigated as DFT in different environments were performed using Spartan'08 program. Density functional theory (DFT), Beck's (B)[20] three-parameter hybrid model, Lee, Yang and Parr's (LYP)[21] optimizing functional correlation, thermal and thermal values under a 6-311G basis set and used to predict. Frontier molecular orbital features, HOMO (highest occupied molecular orbital) and LUMO (lowest unoccupied molecular orbital) were counted at the same theory level.

Molecular Docking Studies

Schrödinger 2021-2 software program[22] was used for ligand preparation, protein preparation and determination of ligand-target interactions in molecular docking. The method part of the molecular docking study was applied in previous studies.[8k,l,23] The reason why **3aa** compound is used as ligand *in silico* approaches is because it has given the best results against anti-cancer experimentally. In molecular docking, compound **3a** was targeted by EGFR and VEGR-2 receptors, which are important in anticancer. Crystal structures of PDB ID:1 M17[14] for EGFR and PDB ID:2RL5 for VEGFR-2 were downloaded from the protein database.

ADMET Prediction

ADME properties were calculated with Schrödinger's QikProp[24] module. All synthesized compounds were subjected to estimations of absorption, distribution, metabolism, excretion (ADME) using the QikProp tool of the Schrödinger package.[24] Calculations of ADME parameters such as QPlogBB, QPlogPo/w, QPlogS, QPlogHERG, QPPCaco, QPPMDCK, QPlogKhsa logarithm were performed.

Supporting Information Summary

Supplementary data (^{1}H NMR & ^{13}C NMR and IR spectra of the synthesized compounds) associated with this article can be found, in the online version, at DOI: 10.1002/slct.202300910

Acknowledgements

Authors would like to thank Erzincan Binali Yıldırım University Research Fund for financial support with project number FBA-2021-762.The authors would like to thank Erzincan Binali Yıldırım University, Basic Sciences Application and Research Center (EBYU-EUTAM) for the Schrödinger Maestro 2021-2 program. The authors would like to thank Assoc. Prof. Azime Berna Özçelik for HRMS analysis. SA would like to thank Suleyman Demirel University Research Fund for financial support with project number TSG-2021-8458.

Conflict of Interests

The authors declare no conflict of interest.

Data Availability Statement

The data that support the findings of this study are available in the supplementary material of this article.

Keywords: 3(2*H*)pyridazinone · cytotoxic activity · DFT · molecular docking · piperazine

[1] a) D. Hanahan, R. A. Weinberg, *Cell* **2011**, *144*, 646–674; b) T. A. Wallace, D. N. Martin, S. Ambs, *Carcinogenesis* **2011**, *32*, 1107–1121; c) T. Pradhan, O. Gupta, G. Singh, V. Monga, *Eur. J. Med. Chem.* **2021**, *221*, 113495; d) X. Yuan, Q. Yang, T. Liu, K. Li, Y. Liu, C. Zhu, Z. Zhang, L. Li, C. Zhang, M. Xie, J. Lin, J. Zhang, Y. Jin, *Eur. J. Med. Chem.* **2019**, *179*, 147–165.

[2] a) M. A. Abdelgawad, R. B. Bakr, W. Ahmad, M. M. Al-Sanea, H. A. H. Elshemy, *Bioorg. Chem.* **2019**, *92*, 103218; b) X. Liang, Q. Wu, S. Luan, Z. Yin, C. He, L. Yin, Y. Zou, Z. Yuan, L. Li, X. Song, M. He, C. Lv, W. Zhang, *Eur. J. Med. Chem.* **2019**, *171*, 129–168.

[3] K. C. Thandra, A. Barsouk, K. Saginala, J. S. Aluru, A. Barsouk, *Contemp Oncol (Pozn)* **2021**, *25*, 45–52.

[4] a) C. Fitzmaurice, D. Abate, N. Abbasi, H. Abbastabar, F. Abd-Allah, O. Abdel-Rahman, A. Abdelalim, A. Abdoli, I. Abdollahpour, A. S. M. Abdulle, N. D. Abebe, H. N. Abraha, L. J. Abu-Raddad, A. Abualhasan, I. A. Adedeji, S. M. Advani, M. Afarideh, M. Afshari, M. Aghaali, D. Agius, S. Agrawal, A. Ahmadi, E. Ahmadian, E. Ahmadpour, M. B. Ahmed, M. E. Akbari, T. Akinyemiju, Z. Al-Aly, A. M. Al Abdul Kader, F. Alahdab, T. Alam, G. M. Alamene, B. T. T. Alemnew, K. A. Alene, C. Alinia, V. Alipour, S. M. Aljunid, F. A. Bakeshei, M. A. H. Almadi, A. Almasi-Hashiani, U. Alsharif, S. Alsowaidi, N. Alvis-Guzman, E. Amini, S. Amini, Y. A. Amoako, Z. Anbari, N. H. Anber, C. L. Andrei, M. Anjomshoa, F. Ansari, A. Ansariadi, S. C. Y. Appiah, M. Arab-Zozani, J. Arabloo, Z. Arefi, O. Aremu, H. A. Areri, A. Artaman, H. Asayesh, E. T. Asfaw, A. F. Ashagre, R. Assadi, B. Ataeinia, H. T. Atalay, Z. Ataro, S. Atique, M. Ausloos, L. Avila-Burgos, E. Avokpaho, A. Awasthi, N. Awoke, B. P. Ayala Quintanilla, M. A. Ayanore, H. T. Ayele, E. Babaee, U. Bacha, A. Badawi, M. Bagherzadeh, E. Bagli, S. Balakrishnan, A. Balouchi, T. W. Bärnighausen, R. J. Battista, M. Behzadifar, M. Behzadifar, B. B. Bekele, Y. B. Belay, Y. M. Belayneh, K. K. S. Berfield, A. Berhane, E. Bernabe, M. Beuran, N. Bhakta, K. Bhattacharyya, B. Biadgo, A. Bijani, M. S. Bin Sayeed, C. Birungi, C. Bisignano, *JAMA Oncol* **2019**, *5*, 1749–1768; b) H. Sung, J. Ferlay, R. L. Siegel, M. Laversanne, I. Soerjomataram, A. Jemal, F. Bray, *Ca-Cancer J. Clin.* **2021**, *71*, 209–249.

[5] a) R. L. Siegel, K. D. Miller, A. Goding Sauer, S. A. Fedewa, L. F. Butterly, J. C. Anderson, A. Cercek, R. A. Smith, A. Jemal, *Ca-Cancer J. Clin.* **2020**, *70*, 145–164; b) D. Duarte, N. Vale, *Drug Discovery Today* **2022**, *27*, 165–184; c) A. Young, D. Rea, *Bmj* **2000**, *321*, 1278–1281.

[6] a) Z. Mao, X. Zheng, Y. Qi, M. Zhang, Y. Huang, C. Wan, G. Rao, *RSC Adv.* **2016**, *6*, 7723–7727; b) A. M. Waszkielewicz, A. Gunia, N. Szkaradek, K. Pytka, A. Siwek, G. Satała, A. J. Bojarski, E. Szneler, H. Marona, *Bioorg. Med. Chem. Lett.* **2013**, *23*, 4419–4423; c) Y. Hori, K. Ishii, H. Kanda, Y. Iwamoto, K. Nishikawa, N. Soga, H. Kise, K. Arima, Y. Sugimura, *Cancer Prev Res (Phila)* **2011**, *4*, 87–96; d) H. Chen, X. Liang, F. Xu, B. Xu, X. He, B. Huang, M. Yuan, *Molecules* **2014**, *19*, 12048–12064; e) H. Chen, F. Xu, X. Liang, B. B. Xu, Z. L. Yang, X. L. He, B. Y. Huang, M. Yuan, *Bioorg. Med. Chem. Lett.* **2015**, *25*, 285–287; f) Z. Özdemir, S. Utku, B. Mathew, S. Carradori, G. Orlando, S. Di Simone, M. A. Alagöz, A. B. Özçelik, M. Uysal, C. Ferrante, *J. Enzyme Inhib. Med. Chem.* **2020**, *35*, 1100–1109; g) X. Liang, P. Wu, Q. Yang, Y. Xie, C. He, L. Yin, Z. Yin, G. Yue, Y. Zou, L. Li, X. Song, C. Lv, W. Zhang, B. Jing, *Eur. J. Med. Chem.* **2021**, *220*, 113473; h) J. Singh, V. Kumar, P. Silakari, S. Kumar, *J. Heterocycl. Chem.* **2022**, *60*, 929-949.

[7] a) M. Y. Hamed, A. F. Aly, N. H. Abdullah, M. F. Ismail, *Polycyclic Aromat. Compd.* **2023**, *43*, 2356–2375; b) Y. M. Ali, M. F. Ismail, F. S. M. Abu El-Azm, M. I. Marzouk, *J. Heterocycl. Chem.* **2019**, *56*, 2580–2591.

[8] a) A. Coelho, E. Sotelo, E. Raviña, *Tetrahedron* **2003**, *59*, 2477–2484; b) S. Demirayak, A. C. Karaburun, R. Beis, *Eur. J. Med. Chem.* **2004**, *39*, 1089–1095; c) C. Rubat, P. Coudert, B. Refouvelet, P. Tronche, P. Bastide, J. Bastide, *Chem Pharm Bull (Tokyo)* **1990**, *38*, 3009–3013; d) I. Sircar, R. E. Weishaar, D. Kobylarz, W. H. Moos, J. A. Bristol, *J. Med. Chem.* **1987**, *30*, 1955–1962; e) J. Gil-Longo, M. de los Reyes Laguna, I. Verde, M. E. Castro,

© 2023 Wiley-VCH GmbH

F. Orallo, J. A. Fontenla, J. M. Calleja, E. Ravina, C. Teran, *J. Pharm. Sci.* **1993**, *82*, 286–290; f) A. Akahane, H. Katayama, T. Mitsunaga, T. Kato, T. Kinoshita, Y. Kita, T. Kusunoki, T. Terai, K. Yoshida, Y. Shiokawa, *J. Med. Chem.* **1999**, *42*, 779–783; g) D. G. Livermore, R. C. Bethell, N. Cammack, A. P. Hancock, M. M. Hann, D. V. Green, R. B. Lamont, S. A. Noble, D. C. Orr, J. J. Payne, *J. Med. Chem.* **1993**, *36*, 3784–3794; h) W. Malinka, A. Redzicka, O. Lozach, *Farmaco* **2004**, *59*, 457–462; i) W. Akhtar, M. Shaquiquzzaman, M. Akhter, G. Verma, M. F. Khan, M. M. Alam, *Eur. J. Med. Chem.* **2016**, *123*, 256–281; j) İ. BozbeyMerde, G. T. Önel, B. Türkmenoğlu, Ş. Gürsoy, E. Dilek, *ChemistrySelect* **2022**, *7*, e202202446; k) İ. B. Merde, G. T. Önel, B. Türkmenoğlu, Ş. Gürsoy, E. Dilek, *Med. Chem. Res.* **2022**, *31*, 2021–2031; l) İ. B. Merde, G. T. Önel, B. Türkmenoğlu, Ş. Gürsoy, E. Dilek, A. B. Özçelik, M. Uysal, *ChemistrySelect* **2022**, *7*, e202201606; m) İ. Bozbey Merde, G. Taşkor Önel, B. Türkmenoğlu, Ş. Gürsoy, E. Dilek, *Fabad Journal of Pharmaceutical Sciences* **2022**, *47(3)*, 355–368; n) Ö. Çöl, İ. Bozbey Merde, B. Türkmenoğlu, M. Uysal, *J. Mol. Struct.* **2022**, *1261*, 132970; o) İ. Bozbey Merde, G. Taşkor Önel, B. Türkmenoğlu, Ş. Gürsoy, E. Dilek, M. Ergün, A. Özçelik, M. Uysal, *J. Res. Pharm.* **2022**, *26(5)*, 1461–1471.

[9] B. J. Deppmeier, A. J. Driessen, T. S. Hehre, W. J. Hehre, J. A. Johnson, P. E. Klunzinger, Y. Jianguo, *Irvine, CA Wavefunction Inc.* **2009**.

[10] a) A. Azazi, A. Mabrouk, K. Alimi, *Comput. Theor. Chem.* **2011**, *978*, 7–15; b) N. Elgrishi, K. J. Rountree, B. D. McCarthy, E. S. Rountree, T. T. Eisenhart, J. L. Dempsey, *J. Chem. Educ.* **2018**, *95*, 197–206.

[11] I. Bozbey, H. Uslu, B. Türkmenoğlu, Z. Özdemir, A. Karakurt, S. Levent, *J. Mol. Struct.* **2022**, *1251*, 132077.

[12] S. Saravanan, V. Balachandran, *Spectrochim. Acta Part A* **2014**, *120*, 351–364.

[13] a) R. G. Parr, L. v. Szentpály, S. Liu, *J. Am. Chem. Soc.* **1999**, *121*, 1922–1924; b) M. Brinzei, A. Stefaniu, O. Iulian, O. Ciocirlan, *Chem. Proc.* **2020**, *3*, 56.

[14] J. Stamos, M. X. Sliwkowski, C. Eigenbrot, *J. Biol. Chem.* **2002**, *277*, 46265–46272.

[15] D. S. La, J. Belzile, J. V. Bready, A. Coxon, T. DeMelfi, N. Doerr, J. Estrada, J. C. Flynn, S. R. Flynn, R. F. Graceffa, S. P. Harriman, J. F. Larrow, A. M. Long, M. W. Martin, M. J. Morrison, V. F. Patel, P. M. Roveto, L. Wang, M. M. Weiss, D. A. Whittington, Y. Teffera, Z. Y. Zhao, A. J. Polverino, J. C. Harmanget, *J. Med. Chem.* **2008**, *51*, 1695–1705.

[16] Q. Xu, Y. Wang, J. Xu, M. Sun, H. Tian, D. Zuo, Q. Guan, K. Bao, Y. Wu, W. Zhang, *ACS Med. Chem. Lett.* **2016**, *7*, 1202–1206.

[17] M. Gökçe, G. Bakir, M. F. Sahin, E. Küpeli, E. Yeşilada, *Arzneim.-Forsch.* **2005**, *55*, 318–325.

[18] a) S. Akkoc, *ChemistrySelect* **2019**, *4*, 4938–4943; b) S. Akkoc, *Synthetic Commun* **2019**, *49*, 2903–2914.

[19] a) B. Turkmenoglu, Y. Guzel, *Comput. Biol. Chem.* **2018**, *76*, 327–337; b) B. Turkmenoglu, Y. Guzel, E. M. Su, D. S. Kizilcan, *Mater. Today Commun.* **2020**, *25*.

[20] A. D. Becke, *Phys. Rev. A* **1988**, *38*, 3098.

[21] C. Lee, W. Yang, R. G. Parr, *Phys. Rev. B* **1988**, *37*, 785.

[22] S. Schrödinger, *Release 2021–2: Glide*, LLC, New York, NY, **2021**.

[23] B. Kuzu, C. Hepokur, B. Turkmenoglu, S. Burmaoglu, O. Algul, *Future Med. Chem.* **2022**, *14*, 1027–1048.

[24] L. Schrödinger, *Release 2021-2: Qikprop*, New York, NY, **2021**.

Submitted: March 9, 2023
Accepted: June 7, 2023

© 2023 Wiley-VCH GmbH

23656549, 2023, 25, Downloaded from https://chemistry-europe.onlinelibrary.wiley.com/doi/10.1002/slct.202300910 by Erzincan Universitesi, Wiley Online Library on [10/07/2023]. See the Terms and Conditions (https://onlinelibrary.wiley.com/terms-and-conditions) on Wiley Online Library for rules of use; OA articles are governed by the applicable Creative Commons License